JOTCS A
Journal of the Turkish Chemical Society
Section: A
Chemistry
TURKISH CHEMICAL SOCIETY

Poly(MMA-co-MI) Nanocomposite with Modified Nano ZRP with KH570 Linker: Preparation, Characterization and Transparency Properties

Fariborz Atabaki*[1], Gholam Ali Koohmareh[2] and Samira Sarikhani[1]
[1]Department of Chemistry, College of Science, Malek-ashtar University of Technology, Isfahan, Iran.
[2]Department of Chemistry, University of Isfahan, Isfahan, 81746-73441, Iran.

Abstract: In this study, zirconium phosphate was synthesized and modified with KH570 linker. It was then used to prepare several nanocomposites with different percent with poly (methyl methacrylate-co-N-2-methyl-4-nitro-phenylmaleimide) (Poly (MMA-co-MI)). The synthesized compounds were characterized by Fourier transform infrared spectroscopy (FTIR), X-ray diffraction (XRD), and field-emission scanning electron microscopy (FE-SEM). The particles size and structure determining showed nanoparticle are sheet and about 9-20 nm. Thermal stability of these compounds were evaluated by thermogravimetric analysis (TGA). The results showed adding nanoparticles to copolymer increased starting weight lost about 20 °C and finishing weight lost about 90 °C. The results of differential scanning calorimetry (DSC), showed that adding nanoparticles decreased the glass transition temperatures (T_g) of the copolymer. The transparency of these nanocomposites were examined by ultraviolet–visible (UV–Vis) spectroscopy. The results showed the best transparency refer to nanocomposites 0.5 to 1% of nanoparticles.

Keywords: Inorganic material, nanocomposite, synthesis of Zirconium nano particle, transparency.

Submitted: March 14, 2022. **Accepted:** May 05, 2022.

Cite this: Atabaki F, Koohmareh GA, Sarikhani S. Poly(MMA-co-MI) Nanocomposite with Modified Nano ZRP with KH570 Linker: Preparation, Characterization and Transparency Properties. JOTCSA. 2022;9(3):809–20.

DOI: https://doi.org/10.18596/jotcsa.1086707.

***Corresponding author E-mail:** atabaki@mut_es.ac.ir, f.atabaki@gmail.com.

INTRODUCTION

The use of polymer nanocomposites has been recently paid much attention to applied and industrial researches. The polymeric matrices and nano fillers in nanocomposite structure have a special importance in determining their features and applications. Since the nanotechnology has been utilized to create materials with improving mechanical and physical properties, nanoparticles were added into the base of materials to form composite materials with unique physical and mechanical properties (1,2), such as the properties of polymers such as flexibility, optical clarity, and excellent dimensional stability of poly methyl methacrylate (PMMA), whereas inorganic materials show mechanical strength, thermal stability, and a high modulus (3-5).

PMMA is one of the common medical polymers employed widely in manufacturing various implants, especially in the fabrication of an ophthalmic intraocular lenses due to its mechanical properties, mould ability, and optical rehabilitation (6,7). Methyl methacrylate (MMA) has been used as a comonomer in several reports such as block copolymer with styrene (6,8,9), copolymerization with tricyclodecyl methacrylate (10), and copolymerization reaction with maleimide (11,12). In addition, the use of PMMA in the preparation of various nanocomposites with several additives such as SiO_2 (13), Clay (14), TiO_2 (15), ZrO_2 (16), MWCNT (17), and Al_2O_3 (18) has been reported.

The use of TiO_2 thin-films with high transmittance in the visible region as antibacterial coating could be effective for PMMA in ophthalmic applications (19,20). It was used with ZrO_2 nano particle for denture base applications, too (7,21) .

Inorganic hybrid nanoparticles are highly attractive in both academic and industrial researches. They are able not only to combine the properties of both components, polymers and inorganic matter, but also provide unique and tuneable properties (22,23). One of the major issues in these materials is dispersing degree of particles into the polymer matrix and the interfacial property between the organic and inorganic components (24,25).

In order to enhance the stability of nanoparticles in the polymer matrix, surface modification of the nanoparticles is needed. It could be improved by introducing coupling agents or reactive functional groups onto the surface of nanoparticles (26).

Zirconium phosphate (ZrP) serves as nano filler in the polymeric interface, where their presence affects profoundly the chemical, mechanical, and thermal properties of the nanocomposite. It is acidic, inorganic cation exchange materials which usually presents a layered structure. There are various phases of ZrP that differ in their interlamellar spaces and their crystalline structure. Among all the ZrP phases, the most widely used are the α-phase and the γ-phase, whose crystal structures were elucidated by Clearfield and co-workers (27). Yamanaka and Hattori reported a mixed ɣ-zirconium phosphate (ɣ-ZrP) benzene phosphonate can be obtained by contacting ɣ-ZrP with benzene phosphoric acid. However, at that time ɣ-ZrP was formulated as $Zr(HPO_4)_2.2H_2O$ and its structure was believed erroneously to be similar to that of α-ZrP but with a different packing of the layers, so it was not possible to give a correct interpretation in order to experimental data (28). While layered ZrP micro-crystals might not be as ideal as porous materials, because of small hydroxyl accessibility, single-layer ZrP nano sheets from the exfoliation of its micro-crystals serve as an ideal candidate for post-grafting since after exfoliation, the hydroxyl groups are fully exposed and readily react with silane. The hydroxyl groups exist on both sides of nano sheets. After surface grafting, the obtained compounds are expected to possess a high density of functional groups, which are critical for high catalytic performance. Furthermore, the lateral dimension of ZrP nano sheets can be altered by tuning the synthetic conditions. Another major advantage of using ZrP nano sheets as the solid substrate is nano sheets can be uniformly dispersed in a wide range of polar solvents, leading to high catalytic efficiency, but meanwhile they can be easily separated from the dispersion system using centrifugation (29).

Modified silica nano particles -3-methacryloxypropyltrimethoxysilane- (KH-570 linker) can be attached to metallic surface by a condensation reaction resulting in a covalent bond and also cause a good interaction with PMMA to preparing nanocomposite (5). As N-2-methyl-4-nitro-phenylmaleimide (MI) was added in PMMA matrix to improve its thermal stability in previews work (30), in this research our goal is to modify nano ZrP with KH570 linker and make a nanocomposite based on this modified nanoparticles with poly(MMA-co-MI).

EXPERIMENTAL SECTION

Materials

Zirconium(IV) chloride ($ZrCl_4$, Aldrich), orthophosphoric acid (H_3PO_4, 85%, Aldrich), tetra-n-butylammonium hydroxide (TBA, Aldrich), nitric acid (Aldrich), KH-570 linker (γ-methacryloyloxypropyl trimethoxy silane, Aldrich), methyl methacrylate (Merck). Benzoyl peroxide (BPO, Merck), 2-methyl-4-nitroaniline (Merck), maleic anhydride (MA, Merck), ethyl acetate, and methanol were distilled over potassium hydroxide under vacuum.

Preparation of N-2-methyl-4-nitro-phenylmaleimide

MI was prepared according to our previous research (30). First, maleic anhydride (4.9 g, 0.05 mol) was dissolved in 15 mL of acetone. Then, a solution of 2-methyl-4-nitroaniline (7.6 g, 0.05 mol) in 15 mL of acetone was added dropwise under vigorous stirring. After complete addition, the mixture is stirred for 1 h. The solid (maleamic acid) which precipitated was filtered off (11.1 g, 89%, mp: 169-171 °C). Maleamic acid (10.0 g, 0.04 mol) was then dissolved in 15 mL of acetic anhydride with added 0.3 g of sodium acetate. The mixture was heated for 6 h under reflux. A cream solid is recovered (8.64 g, 93%. mp: 251–253 °C).

Preparation of Nanoparticle

In order to modify ZrP with KH-570 linker, first ZrP was synthesized and exfoliated with TBA according to reported procedures. It was then modified with KH-570 linker (Scheme 1).

Preparation of zirconium phosphate (31,32)

Zirconium tetrachloride (4.66 g, 20 mmol) was dissolved in water (25 mL) and heated 100 °C, to make a saturated 2 M zirconium solution. Upon cooling, Zirconium oxychloride crystals (5.51 g, yield: 85.3%, mp: 149-152 °C) were formed. Zirconium oxychloride (5 g) was mixed with 50 mL of 6.0 M orthophosphoric acid solution in demineralized water (DMW) at 25 °C for 1 h and at 80 °C for 24 h. The precipitate was collected, followed by washing with DMW, and drying for 24 h in oven at 80 °C. This product was then treated with 20 mL (0.1 M) nitric acid solution for complete replacement of counter ions with H^+ ions at 25 °C for 1 h and was washed with DMW (7.12 g, yield:71.4%)

Reaction of ZrP with TBA (29)

The prepared ZrP (2.2 g in 10 mL of water) was reacted and exfoliated with TBA (10 mL of 0.5 M aqueous solution) in an ice bath for 6 h and at 25 °C for 18 h. The precipitate was smoothed and dried at 25 °C (1.8 g, yield: 81.8%, decomposed at 311 °C)

Modification of exfoliated ZrP with KH-570 linker

A solution of KH-570 linker (1 mL in 10 ml HCl 0.1 M) was added to a solution of exfoliated ZrP (1 g, in 5 mL of water) and spired at 65 °C for 1 h. The precipitate was collected (0.94 g, yield: 95.9%, mp>293 °C, XRF data acquired from the analyzer is (P, 18.2; Zr, 21.4; other 57.7), other is for elements smaller than Na such as C, O, H, Si; and calculated elemental analysis for $(ZrOPO(OH)OSi(OMe)_2(CH_2)_3OCOCCH_3CH_2)OPO(OH)_2)$ is (C, 20.89; H, 3.90; O, 40.19; P, 11.97; Si, 5.43; Zr, 17.63).

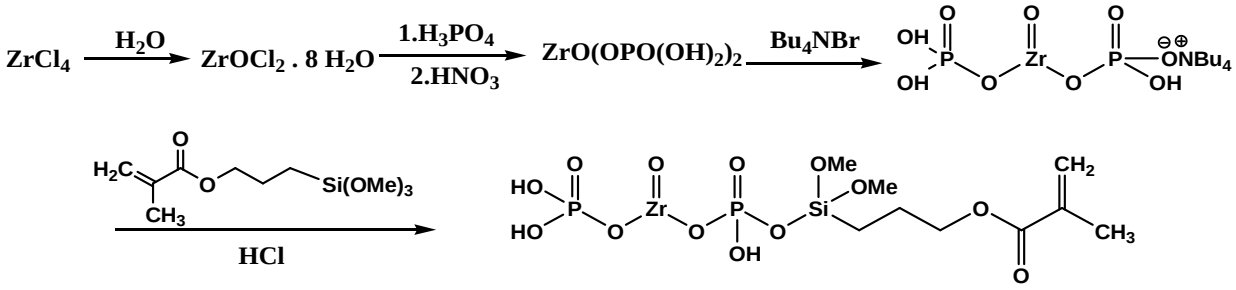

Scheme 1.

Synthesis of poly (MMA-co-MI)

In a 250 mL round bottomed flask, equipped with reflux condenser and nitrogen inlet tube, a solution of MMA (1.1 mL, 10 mmol), and MI (1 gr, 0.4 mmol) in ethyl acetate (6 mL) was prepared. BPO (0.02 g) was added and the reaction mixture was heated for 8h at 77 ºC (reflux). The solution was then poured in methanol and the precipitate was washed with methanol and dried. (1.8 gr, yield: 85.7%, CHNS data acquired from the analyzer is (C, 58.49; H, 6.04; N, 5.58), and calculated elemental analysis for predicted copolymer is (C, 58.36; H, 5.91; N, 6.01; O, 29.73). Percentage of MI in copolymer is 27.8% (Scheme 2).

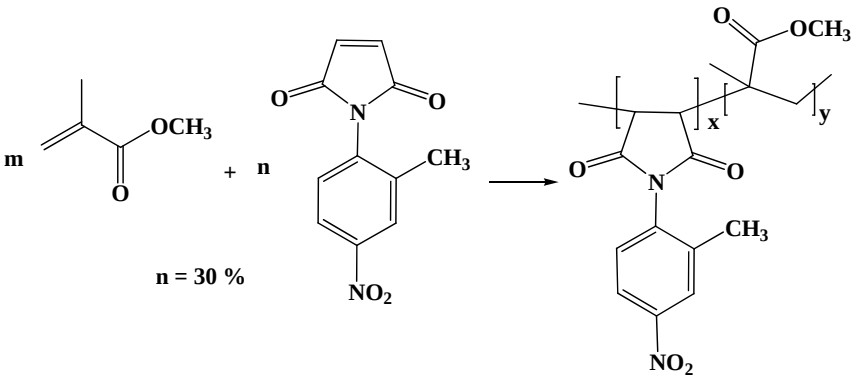

Scheme 2.

Preparation of Nanocomposite

A solution of synthesized copolymer (1 g) in ethyl acetate (10 mL) was prepared. A dispersion of modified nanoparticles (0.01 g) in ethyl acetate (5 mL) was sonicated for 20 min and was added to a prepared polymer solution and sonicated again for 20 min. The solution was then precipitated in methanol to afford 1% nanocomposite powder. Four other percentages were prepared according to the same procedure. In other reaction experiments, an in-situ nanocomposites were prepared by adding the appropriate nanoparticle amounts into monomers mixtures during polymerization reaction.

Characterization

FT-IR spectral data were recorded with a Bruker spectrometer in the range of 4000–400 cm^{-1} using KBr disks. SEM image of the electrospinning nanofibers was obtained through the scanning electron microscopy (SEM). The morphology of the pristine α-ZrP powder was also observed at an accelerating voltage of 5 kV. The chemical state of the surface was characterized by X-ray photoelectron spectroscopy Bruker model D8ADVANCE. TEM micrographs were obtained with an H-7500 transmission electron microscope (Philips 208 S 100 kW) at an accelerating voltage of 75 kV. Ultrathin sections were microtome at room temperature. Thermal stabilities were measured via thermogravimetric analysis in nitrogen with a TA Instruments model Q2000 at a heating rate of 20 ˚C min^{-1}. DSC was used to measure glass transition temperature using a TA Q2000 instrument in nitrogen atmosphere at the heating rate of 20 ˚C/min from 80 to 150 C and a cooling rate of 10 ˚C/min. The adsorption ability of Poly (MMA-co-MI)/nano (ZrP-KH570) was investigated by solution adsorption technique. For measuring transmittance in UV and visible area, 50 mg of nanocomposite was dissolved in 10 mL ethyl acetate, Ultraviolet-visible spectrophotometer model Photonix Ar 2015 was used. X-Ray Fluorescence analysis (XRF) was determined with XRF device model Niton from Thermo Company. Elemental analyses (CHNS) was determined by device model Vario EL Ш from Elementar Company.

RESULTS AND DISCUSSION

Characterization

Modified ZrP with KH-570 was prepared according to Scheme 1. FTIR spectra of these compounds are illustrated in Figure 1. For ZrP, the peaks locating at 3594, 3510 are due to the water molecules in the interlayer space of ZrP, 3164, and 1620 cm^{-1} are assigned as symmetric and bending vibrations of –

OH groups, respectively (29). The peaks at 3384, 1251 968 cm^{-1} are attributed to P–OH stretching vibrations or deformation vibrations. The strong bands in the range of 1000–1200 cm^{-1} are characteristic of PO_4 stretching vibrations and 597 cm^{-1} is ascribed to the vibration of Zr−O (33). After reaction of ZrP with TBA, no significant change was occurred and just the P-OH at 1200 cm^{-1} become broader, which was due to the presence of ammonium salt. After modification with KH-570 linker, a peak at 1745 cm^{-1} was appeared and confirmed presence of carbonyl group in the particles and 2957 cm^{-1} is ascribed to the asymmetric C–H stretching of SiOMe and The peaks at 980 cm^{-1} is attributed to C=C bending (34).

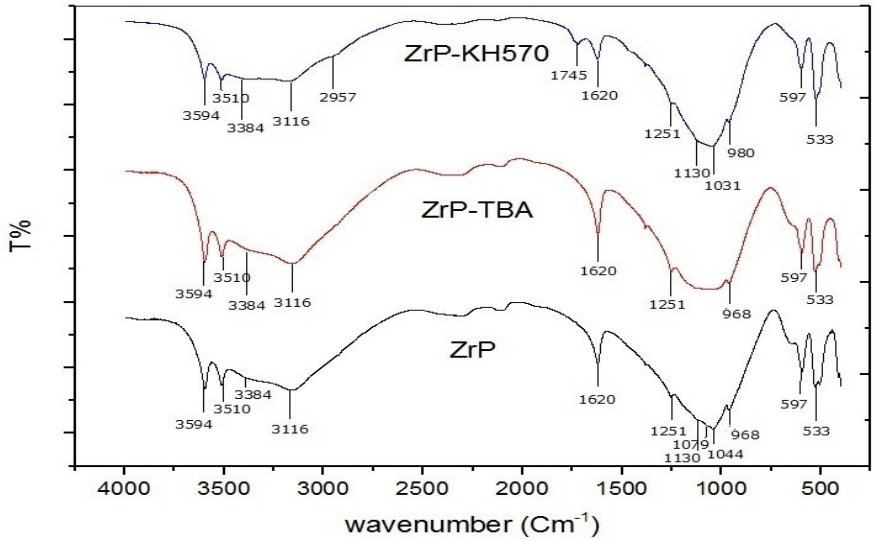

Figure 1: FTIR spectra of ZrP nano particles, ZrP modified by TBA and ZrP modified by KH-570 linker.

Solution polymerization of MMA with synthesized MI was led to poly (MMA-co-MI) due to Scheme 2. It was then sonicated with modified ZrP with KH-570 to prepare the related nanocomposites. Evaluation of the best technique for preparation of nanocomposite an in situ preparation during polymerization was also investigated. All of the polymers and composites were investigated using FTIR spectroscopy. (Figure 2).

The peaks of C=O (1727 cm^{-1}), CH3–O (1148, 1194 cm^{-1}), and C–O (1242, 1270 cm^{-1}) are consistent with those of PMMA as reported in the literature (35,36). And also the bands at 1782 cm^{-1} (C=O imide stretching), 1589 cm^{-1} (C=C aromatic stretching), 1530 and 1348 cm^{-1} (N=O stretching) show the maleimide units as mentioned in the literature and also peaks of nano particle that is discussed in Figure 1 (30,37,38).

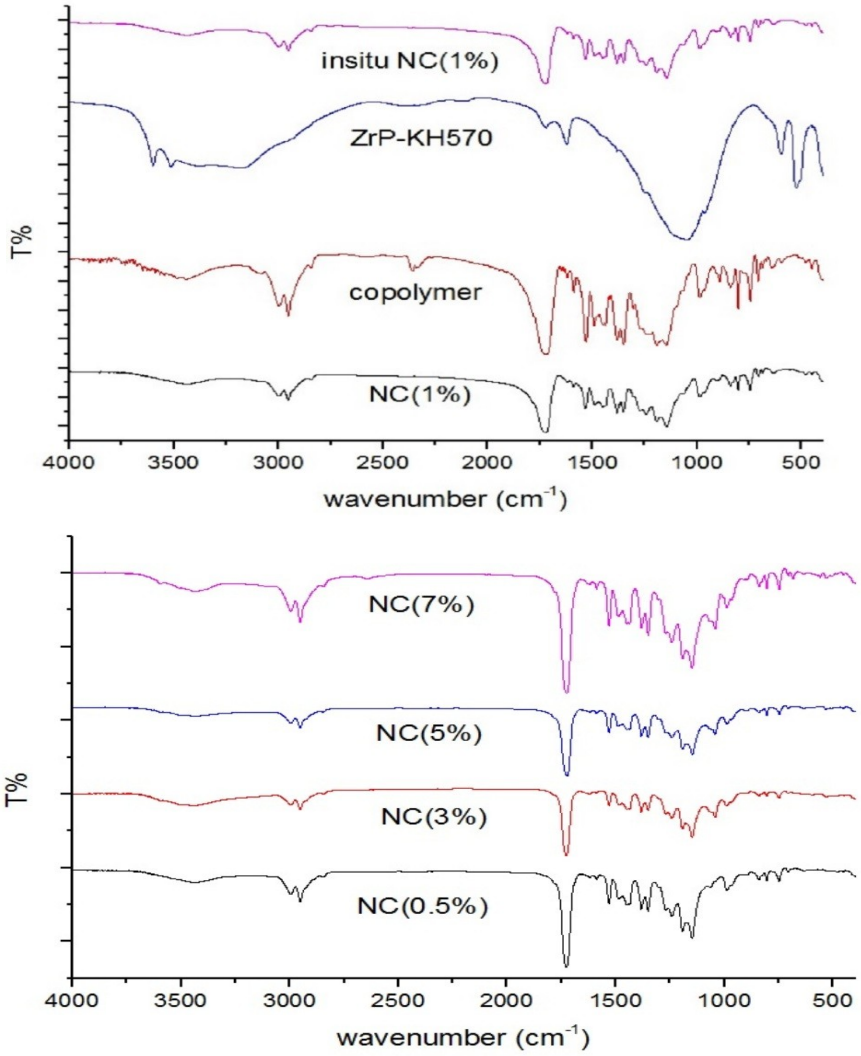

Figure 2: FTIR spectra of poly (MMA-co-MI)–ZrP nanocomposites, poly (MMA-co-MI).

XRD analysis: It is known that ZrP has a clay-like layered structure, which can be characterized using XRD, with interlayer separation calculated from the Bragg equation. Figure 3(a–d) presents the XRD results. Sharpening the peaks of Figure 3b confirms the preparation of ammonium salts of nanoparticles compared to the peaks of Figure 3a. As shown in Figure 3d nanocomposite have both nanoparticles and PMMA background peak (39). The diffractogram of ZrP sample shows peaks at 2θ values: 7, 14, 23, 29, 40, 44, and 56. Reacted ZrP with TBA's spectrum shows same peaks, with a large difference in peak wide at 2θ: 7. Modified ZrP by KH-570's spectrum shows all peaks above except 44. According to Scherrer equation ($D = (0.9\ \lambda)/ (\beta \cos \theta)$) the size of crystals of nano particles can be determined. D is the mean size of the ordered (crystalline) domains, which may be smaller or equal to the particle size. λ is the X-ray wavelength (1.789 A°). β is the line broadening at half the maximum intensity (FWHM) in radian and θ is the Bragg angle. The results are summarized in Table 1 (40).

Table 1: Size of nano particles.

Nanoparticles	ZrP	ZrP-TBA	ZrP-KH
D(nm)	19.13	10.359	9.347
Used 2θ (°)	14	14	14

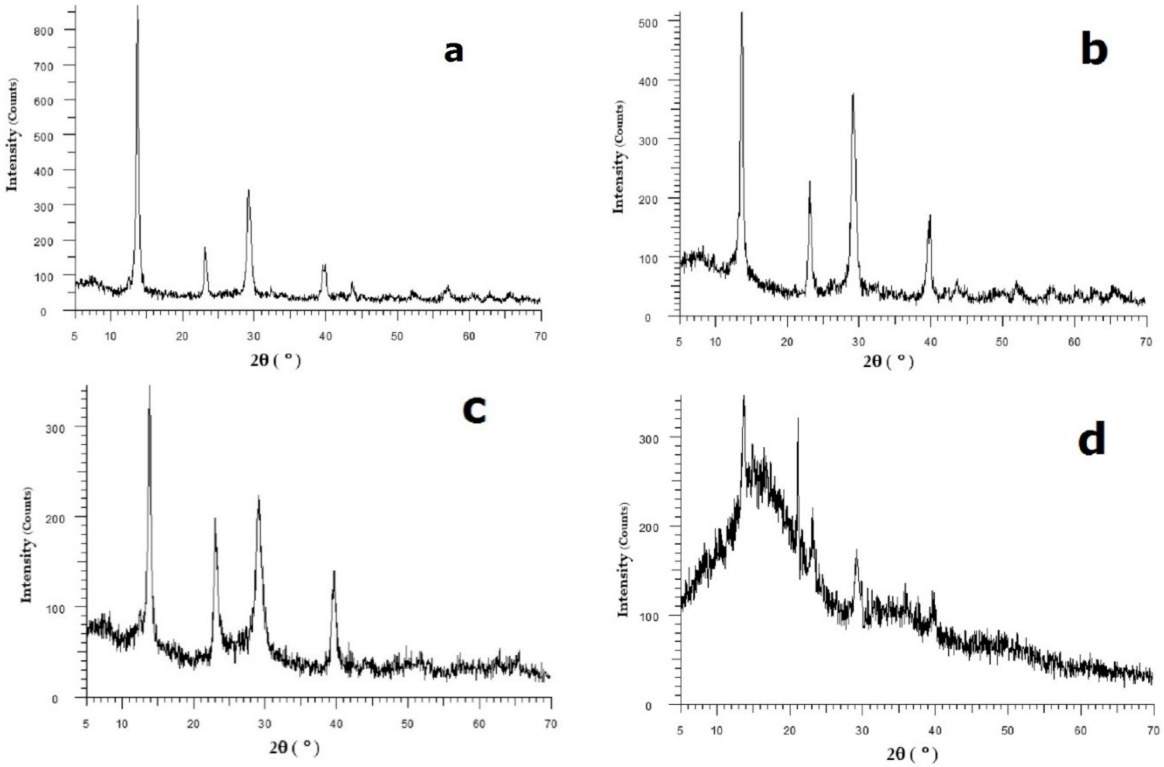

Figure 3: XRD results: (a) ZrP, (b) ZrP modified by TBA, (c) ZrP modified by KH-570 linker, (d) MMA-co-MI/ZrP 1% nanocomposite.

SEM micrographs: Figure 4 shows SEM micrographs of the ZrP modified by KH-570 linker and nanocomposites. Figure 4a confirms modified ZrP crystals sheet structure clearly. Figure 4b-d shows the good dispersion of nanoparticle in polymer layers. Figure 4e shows the undesirable accumulation of nanoparticle in nanocomposite 5%. It can make this composite unsuitable in some properties.

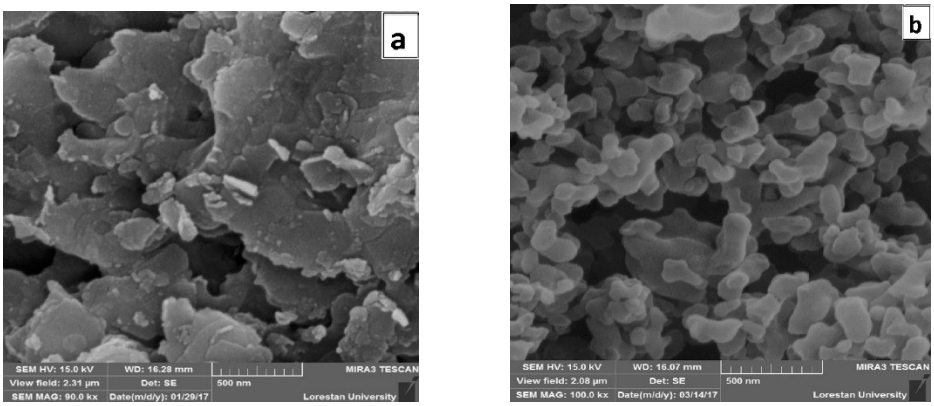

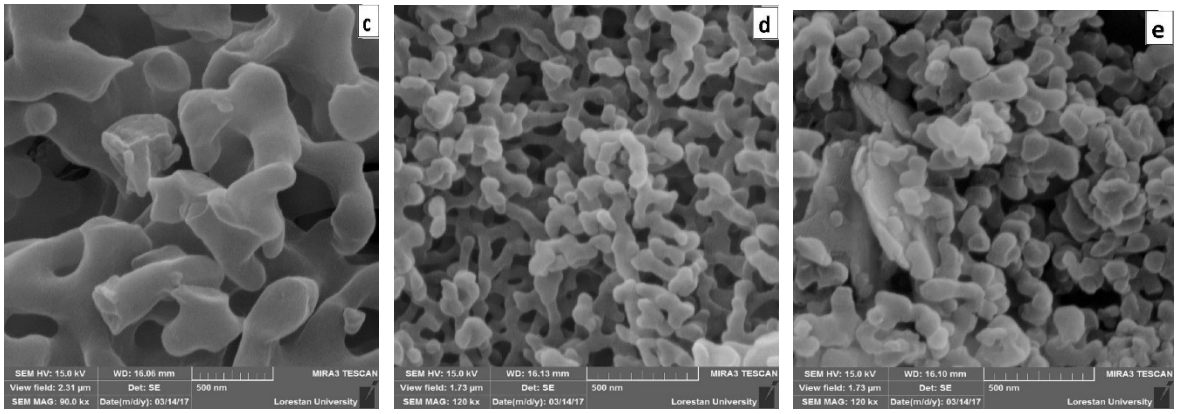

Figure 4: SEM micrographs of pristine ZrP nano particle (a) and poly (MMA-co-MI)/ZrP nanocomposite (b: 0.5%; c; 1%; d: 3%; e: 5%)

TEM micrographs: TEM micrographs of modified nano ZrP and nanocomposite are shown in Figure 5. As seen clearly, nanoparticles are evenly distributed in the polymer matrix.

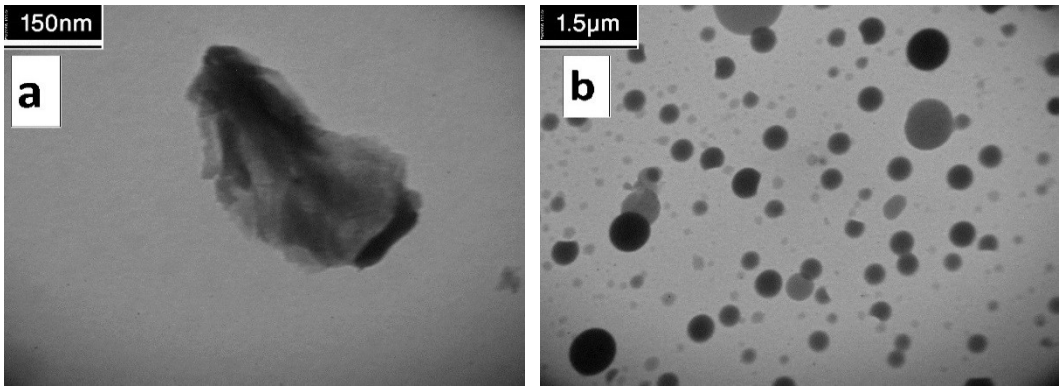

Figure 5: TEM micrographs of (a) modified nano ZrP and (b) poly (MMA-co-MI)/ZrP nanocomposite.

The thermal decomposition of the pristine ZrP and modified ZrP nanoparticle were studied by TGA, DSC, DTG (Figure 6a-c). The range of two major weight losses of the pristine ZrP crystals are 95−170 and 430−590 °C. They refer to the loss of hydration water and condensation water in ZrP, respectively. Three major weight losses in 70−140, 320-440 and 490−600 °C range were observed in the modified ZrP by TBA. They correspond to the loss of hydration water, elimination of TBA and condensation water in ZrP-TBA. Two weight loss steps were observed in 85-185 and 470-620 °C in the modified ZrP by KH-570. First, it refers to the losing water and methoxy group, then losing methacrylate (29,41,42). Nanocomposites thermal properties and behaviour were investigated by TGA and DSC. The results are summarized in Table 2. The T_{10}, T_{50} and T_{max} were highlighted; T_{10} is the onset temperature, at which 10% degradation occurs, while T_{50} is the midpoint temperature, corresponding to 50% degradation. T_{max} is the weight lost finishing temperature. The copolymer start losing weight at around 265 ºC and when nanoparticles were added into its matrix, the temperature increase around 20 ºC for starting weight loss of nanocomposites. The copolymer weight lost finishing around 576 ºC while nanocomposites around 667 ºC. It means improving the thermal stability. Nanocomposite's T_{10}, T_{50}, T_{max} and initiation weight lost temperature are more than PMMA nanocomposite. It shows good improvement of thermal stability nanocomposite than PMMA nanocomposite (43,44).

The eighth column shows time of using in-situ nanoparticles. As seen, adding ZrP nanoparticles to copolymer decrease amount of T_g, but the nanocomposite T_g are higher than PMMA nanocomposite. Also adding nanoparticle during polymerization have more effects on decrease of T_g.

Table 2: Sample designations; T_{max} and T_g of poly (MMA-co-MI)/ZrP-nanocomposite films measured from TGA and DSC curves.

Sample designation	PMMA-ZrP	Copolymer	CP/ZrP-1	CP/ZrP-3	CP/ZrP-5	CP/ZrP-7	In-situ nanocomposite
α-ZrP (w%)	1	0	1	3	5	7	1
$T_{10\%}$	284.5	327.52	328.1	318.02	321.51	318.79	334.7
$T_{50\%}$	367.6	369.96	360.07	360.46	359.11	361.82	378.5
T_{max} (°C)	488.2	576.18	667.6	679.06	669.0	674.22	691.5
T_g (°C)	96.1	133.7	113.85	114.11	115.2	115.35	106.6
Coal Productivity	2.87	15.30	11.51	12.04	15.74	15.09	12.25

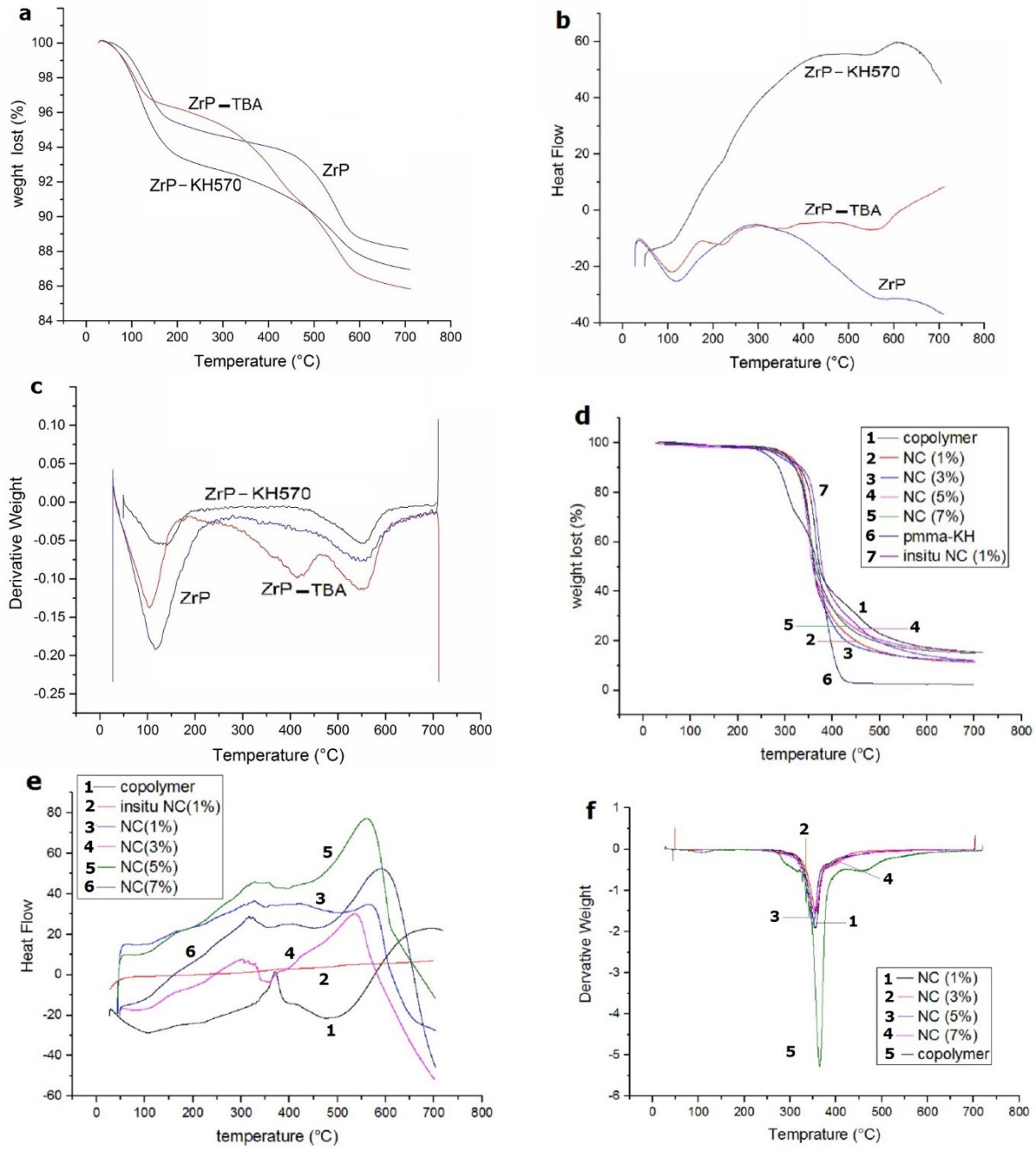

Figure 6: a, b, c are TGA, DSC and DTG of the nanoparticle, respectively. d, e, f are TGA, DSC and DTG of the nanocomposite, respectively.

The transparency of the polymer and prepared nanocomposites were examined by UV-Vis spectroscopy. Figure 7 shows UV-Vis spectra of copolymer and nanocomposite solutions in EtOAc. The transparency of nanocomposite solutions 5 and 7% in 400 nm was about 11% which was not suitable. It reached to 73% that is near the copolymer transparency in nanocomposite solutions (3%). The best transparencies were observed in nanocomposites solutions 0.5, 1%, and in-situ, was 95% in 400 nm. All of the nanocomposites have more transmittance than PMMA nanocomposite except 5, 7%. Since nanocomposites 0.5 and 1% transmit the visible light as well as PMMA, they can be used whenever PMMA is used as a substitute for glass. Furthermore, nanocomposites do not transmit UV light so they can be used in sunglasses.

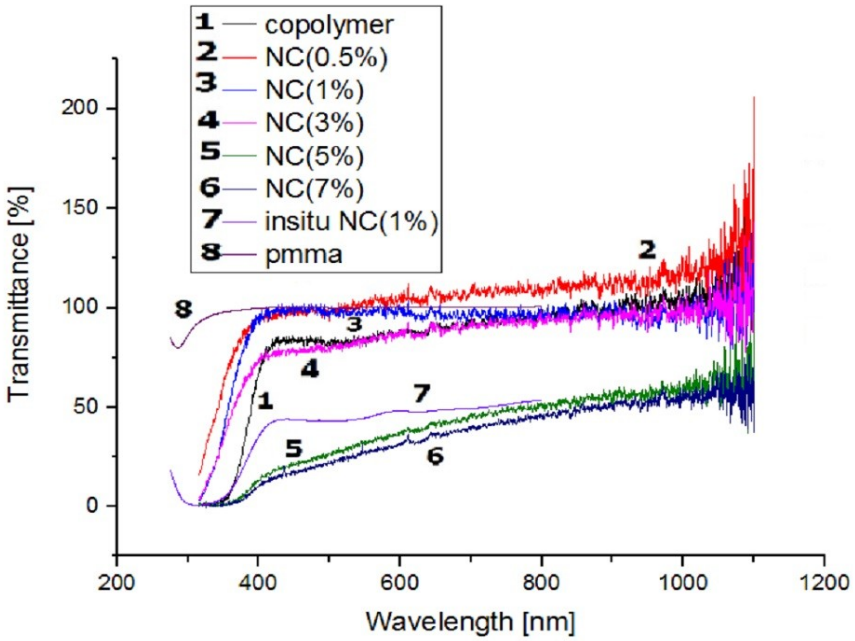

Figure 7: UV-Vis spectra of nanocomposite solutions.

CONCLUSION

A series of nanocomposites based on poly (MMA-co-MI) as a matrix and modified ZrP-KH570 was prepared and characterized by FTIR spectroscopy. The crystalline structure and the size of nanoparticles were confirmed by XRD. The surface morphology of these compounds, evaluated by SEM, were observed as sheet for nanoparticles. It was successfully dispersed in polymer matrix after sonication. The dispersion of nanoparticles into polymer matrix was also confirmed by TEM. Thermal analysis of nanoparticle was investigated.

The thermal stability of nanocomposites was examined by TGA and the results show that adding nanoparticle improve copolymer's thermal stability. Also, thermal behavior of these compounds, evaluated by DSC, shows a decrease in T_g after adding of nanoparticles into polymer matrix. It was probably due to location of nanoparticles between the polymer layers and so decrease interaction between polymer layers.

The results of transparency by UV-Vis spectroscopy showed that the best percent refer to nanocomposite 0.5 and 1% of nanoparticles. Nanocomposites absorb UV light well.

REFERENCES

1. Shafiee Hasani S, Ghazi Tabatabaei Z. Synthesis of Nanocomposites of Single-Wall Carbon Nanotubes Coated with ZnO Nanoparticles in a Matrix of Poly Methyl Methacrylate and Study of Its Optical Properties. Nashrieh Shimi va Mohandesi Shimi Iran. 2019;38(3):23–32.

2. Fatalla AA, Tukmachi MS, Jani GH. Assessment of some mechanical properties of PMMA/silica/zirconia nanocomposite as a denture base material. IOP Conference Series: Materials Science and Engineering. 2020 Nov;987(1):012031. <DOI>.

3. Tucureanu V, Matei A, Mihalache I, Danila M, Popescu M, Bita B. Synthesis and characterization of YAG:Ce,Gd and YAG:Ce,Gd/PMMA nanocomposites for optoelectronic applications. J Mater Sci. 2015 Feb;50(4):1883–90. <DOI>.

4. Singh AK, Prakash R, Pandey D. A comparative thermal, optical, morphological and mechanical properties studies of pristine and C15A nanoclay-modified PC/PMMA blends: a critical evaluation of the role of nanoclay particles as compatibilizers. RSC Adv. 2013;3(35):15411-20. <DOI>.

5. Schoth A, Wagner C, Hecht LL, Winzen S, Muñoz-Espí R, Schuchmann HP, et al. Structure control in PMMA/silica

hybrid nanoparticles by surface functionalization. Colloid Polym Sci. 2014 Oct;292(10):2427–37. <DOI>.

6. Gianotti V, Antonioli D, Sparnacci K, Laus M, Giammaria TJ, Ferrarese Lupi F, et al. On the Thermal Stability of PS- b -PMMA Block and P(S- r -MMA) Random Copolymers for Nanopatterning Applications. Macromolecules. 2013 Oct 22;46(20):8224–34. <DOI>.

7. Ali Sabri B, Satgunam M, Abreeza N, N. Abed A. A review on enhancements of PMMA Denture Base Material with Different Nano-Fillers. Jones IP, editor. Cogent Engineering. 2021 Jan 1;8(1):1875968. <DOI>.

8. Azimi HR, Rezaei M, Majidi F. The non-isothermal degradation kinetics of St–MMA copolymers. Polymer Degradation and Stability. 2014 Jan;99:240–8. <DOI>.

9. Teodorescu M. Free-radical copolymerization of methyl methacrylate with styrene in the presence of 2-mercaptoethanol II. Influence of methyl methacrylate/styrene ratio. European Polymer Journal. 2002 May;38(5):841–6. <DOI>.

10. Lin CT, Kuo SW, Huang CF, Chang FC. Glass transition temperature enhancement of PMMA through copolymerization with PMAAM and PTCM mediated by hydrogen bonding. Polymer. 2010 Feb;51(4):883–9. <DOI>.

11. Gevrek TN, Bilgic T, Klok HA, Sanyal A. Maleimide-Functionalized Thiol Reactive Copolymer Brushes: Fabrication and Post-Polymerization Modification. Macromolecules. 2014 Nov 25;47(22):7842–51. <DOI>.

12. Konsulov V, Grozeva Z, Tacheva J, Tachev K. Study of the copolymerization of n-(dichlorophenyl) maleimides with methyl methacrylate. Bulgarian chemical communications. 2009;41(1):31–8.

13. Sanchez FA, Redondo M, Olmos D, Kuzmanovic M, González-Benito J. A Near-Infrared Spectroscopy Study on Thermal Transitions of PMMA and PMMA/SiO 2 Nanocomposites. Macromol Symp. 2014 May;339(1):48–59. <DOI>.

14. Lerari D, Peeterbroeck S, Benali S, Benaboura A, Dubois Ph. Combining atom transfer radical polymerization and melt compounding for producing PMMA/clay nanocomposites. J Appl Polym Sci. 2011 Aug 5;121(3):1355–64. <DOI>.

15. Hosoda T, Yamada T. Effect of TiO 2 on morphology and mechanical properties of PVDF/PMMA blend films prepared by melt casting process. J Appl Polym Sci. 2014 Jul 5;131(13):1-10. <DOI>.

16. Akinci A, Sen S, Sen U. Friction and wear behavior of zirconium oxide reinforced PMMA composites. Composites Part B: Engineering. 2014 Jan;56:42–7. <DOI>.

17. Zanotto A, Luyt AS, Spinella A, Caponetti E. Improvement of interaction in and properties of PMMA-MWNT nanocomposites through microwave assisted acid treatment of MWNT. European Polymer Journal. 2013 Jan;49(1):61–9. <DOI>.

18. Hazim A, Abduljalil HM, Hashim A. Structural, Spectroscopic, Electronic and Optical Properties of Novel Platinum Doped (PMMA/ZrO2) and (PMMA/Al2O3) Nanocomposites for Electronics Devices. Trans Electr Electron Mater. 2020 Dec;21(6):550–63. <DOI>.

19. Su W, Wang S, Wang X, Fu X, Weng J. Plasma pre-treatment and TiO2 coating of PMMA for the improvement of antibacterial properties. Surface and Coatings Technology. 2010 Oct;205(2):465–9. <DOI>.

20. Yıldırım A, Acay H, Baran A. Synthesis and characterization of the molecularly imprinted composite as a novel adsorbent and its competition with non-imprinting composite for removal of dye. JOTCSA. 2021;8(2):609–22. <DOI>.

21. Zidan S, Silikas N, Alhotan A, Haider J, Yates J. Investigating the Mechanical Properties of ZrO2-Impregnated PMMA Nanocomposite for Denture-Based Applications. Materials. 2019 Apr 25;12(8):1344. <DOI>.

22. Yi C, Yang Y, Liu B, He J, Nie Z. Polymer-guided assembly of inorganic nanoparticles. Chem Soc Rev. 2020;49(2):465–508. <DOI>.

23. Adnan M, Dalod A, Balci M, Glaum J, Einarsrud MA. In Situ Synthesis of Hybrid Inorganic–Polymer Nanocomposites. Polymers. 2018 Oct 11;10(10):1129. <DOI>.

24. Hassanzadeh-Aghdam MK, Ansari R, Mahmoodi MJ, Darvizeh A. Effect of nanoparticle aggregation on the creep behavior of polymer nanocomposites. Composites Science and Technology. 2018 Jul;162:93–100. <DOI>.

25. Hamming LM, Qiao R, Messersmith PB, Catherine Brinson L. Effects of dispersion and interfacial modification on the macroscale properties of TiO2 polymer–matrix nanocomposites. Composites Science and Technology. 2009 Sep;69(11–12):1880–6. <DOI>.

26. Chau JLH, Hsieh CC, Lin YM, Li AK. Preparation of transparent silica–PMMA nanocomposite hard coatings. Progress in Organic Coatings. 2008 Jun;62(4):436–9. <DOI>.

27. Díaz A, Mosby BM, Bakhmutov VI, Martí AA, Batteas JD, Clearfield A. Self-Assembled Monolayers Based Upon a Zirconium Phosphate Platform. Chem Mater. 2013 Mar 12;25(5):723–8. <DOI>.

28. Alberti G, Vivani R, Biswas RK, Murcia-Mascarós S. Preparation and some properties of γ-zirconium phosphate benzenephosphonate. Reactive Polymers. 1993 May;19(1–2):1–12. <DOI>.

29. Zhou Y, Huang R, Ding F, Brittain AD, Liu J, Zhang M, et al. Sulfonic Acid-Functionalized α-Zirconium Phosphate Single-Layer Nanosheets as a Strong Solid Acid for Heterogeneous Catalysis Applications. ACS Appl Mater Interfaces. 2014 May 28;6(10):7417–25. <DOI>.

30. Atabaki F, Abdolmaleki A, Barati A. Free radical copolymerization of methyl methacrylate and N-2-methyl-4-nitro-phenylmaleimide: Improvement in the Tg of PMMA. Colloid Polym Sci. 2016 Feb;294(2):455–62. <DOI>.

31. Carter DP. Preparation of zirconium oxychloride [Internet]. US4256463A.1981 Available from: <URL> .

32. Baig U, Wani WA, Ting Hun L. Facile synthesis of an electrically conductive polycarbazole–zirconium(iv)phosphate cation exchange nanocomposite and its room temperature ammonia sensing performance. New J Chem. 2015;39(9):6882–91. <DOI>.

33. Barraclough C, Bradley D, Lewis J, Thomas I. 510. The infrared spectra of some metal alkoxides,

trialkylsilyloxides, and related silanols. Journal of the Chemical Society (Resumed). 1961;2601–5.

34. Matinlinna JP, Özcan M, Lassila LVJ, Vallittu PK. The effect of a 3-methacryloxypropyltrimethoxysilane and vinyltriisopropoxysilane blend and tris(3-trimethoxysilylpropyl)isocyanurate on the shear bond strength of composite resin to titanium metal. Dental Materials. 2004 Nov;20(9):804–13. <DOI>.

35. Zhang FA, Song C, Yu CL. Effects of preparation methods on the property of PMMA/SBA-15 mesoporous silica composites. J Polym Res. 2011 Nov;18(6):1757–64. <DOI>.

36. Licoccia S, Trombetta M, Capitani D, Proietti N, Romagnoli P, Di Vona ML. ATR–FTIR and NMR spectroscopic studies on the structure of polymeric gel electrolytes for biomedical applications. Polymer. 2005 Jun;46(13):4670–5. <DOI>.

37. Choudhary V, Mishra A. Studies on the copolymerization of methyl methacrylate and N-aryl maleimides. J Appl Polym Sci. 1996 Oct 24;62(4):707–12. <DOI>.

38. Lee SS, Ahn TO. Direct polymer reaction of poly(styrene-co-maleic anhydride): Polymeric imidization. J Appl Polym Sci. 1999 Feb 14;71(7):1187–96. <DOI>.

39. Shobhana E. X-Ray diffraction and UV-visible studies of PMMA thin films. International Journal of Modern Engineering Research. 2012;2(3):1092–5.

40. Patterson AL. The Scherrer Formula for X-Ray Particle Size Determination. Phys Rev. 1939 Nov 15;56(10):978–82. <DOI>.

41. Li X, Wang Z, Wu L, Tsai T. One-step in situ synthesis of a novel α-zirconium phosphate/graphene oxide hybrid and its application in phenolic foam with enhanced mechanical strength, flame retardancy and thermal stability. RSC Adv. 2016;6(78):74903–12. <DOI>.

42. Kozawa Y, Suzuki S, Miyayama M, Okumiya T, Traversa E. Proton conducting membranes composed of sulfonated poly(etheretherketone) and zirconium phosphate nanosheets for fuel cell applications. Solid State Ionics. 2010 Mar 11;181(5–7):348–53. <DOI>.

43. Carvalho HWP, Suzana AF, Santilli CV, Pulcinelli SH. Structure and thermal behavior of PMMA–polysilsesquioxane organic–inorganic hybrids. Polymer Degradation and Stability. 2014 Jun;104:112–9. <DOI>.

44. Hatanaka LC, Diaz A, Wang Q, Cheng Z, Mannan MS. Thermal Stability of Optically Transparent Alpha-Zirconium Phosphate/Poly(methyl methacrylate) Nanocomposites with High Particle Loading. Polymers and Polymer Composites. 2017 May;25(4):267–72. <DOI>.